PERFORMANCE ANALYSIS OF FUZZY MATHEMATICAL MORPHOLOGY OPERATORS ON NOISY MRI

A. BOUCHET[1,2], F. BENALCÁZAR PALACIOS[3,4], M. BRUN[1] and V.L. BALLARIN[1]

[1] *Grupo de Procesamiento Digital de Imágenes, Facultad de Ingeniería, UNMDP, Argentina.*
[2] *Consejo Nacional de Investigaciones Científicas y Técnicas (CONICET).*
[3] *Dpto. de Postgrado, Maestría en Física Médica. Instituto Balseiro.*
[4] *Escuela de Física y Matemática, Facultad de Ciencias, Escuela Superior Politécnica de Chimborazo.*
abouchet@fi.mdp.edu.ar

***Abstract*— Despite a large amount of publications on Fuzzy Mathematical Morphology, little effort was done on systematic evaluation of the performance of this technique. The goal of this work is to compare the robustness against noise of Fuzzy and non Fuzzy Morphological operators when applied to noisy images. Magnetic Resonance Images (MRI) of the brain are a kind of images containing some characteristics that make fuzzy operators an interesting choice, because of their intrinsic noise and imprecision. The robustness was evaluated as the degree in which the results of the operators are not affected by artificial noise in the images. In the analysis we compared different implementation of Fuzzy Mathematical Morphology, and observed that in most of the cases they show higher robustness against noise than the classical morphological operators.**

***Keywords*— Biomedical Images, Digital Image Processing, Mathematical Morphology, Fuzzy Mathematical Morphology.**

I. INTRODUCTION

The theory of Mathematical Morphology (MM) is a powerful tool in the Digital Image Processing field. It is broadly used as a processing tool for enhancement, segmentation, edge detection, filtering, and more generally, the analysis of internal structures (Serra, 1982; Serra, 1988; Ronce and Heijmans, 1991). A key aspect of this theory is the use of the structuring element, a probe set that is used to test the image in several ways, generating information about its geometry. One of the reasons of the success of Mathematical Morphology is its simplicity of implementation: most of the operators can be built by combination of basic operators of negation, complement, dilation and erosion. The last two are considered the pillars of MM, and most of its variants are based on variants of these operators, as for example in the gray level morphology (Bangham and Marshall, 1998).

In the other hand, the theory of Fuzzy Sets is an extension to the classical set theory, allowing for the representation of uncertainty, modeled as degrees of membership (Zadeh, 1965). This theory has been applied with many degrees of success, including control and decision making.

When combined with Mathematical Morphology, Fuzzy Set theory extends the applicability of this model by adding the ability to handle uncertainty. Extension of classical binary MM to gray level images, is obtained via Fuzzy Mathematical Morphology (FMM), which combines the power of Mathematical Morphology, based on set theory, with the ability of fuzzy logic to handle degrees of membership. FMM has been developed in various directions, until it was combined in a unique theoretical framework (De Baets *et al.*, 1995; De Baets *et al.*, 1995; Kerre and Nachtegael, 2000; Bloch and Maître, 1995; Di Gesu *et al.*, 1993).

II. BACKGROUND

Several methodologies have been developed to extend binary MM to grayscale images. One of these extensions, based on fuzzy set theory, is the Fuzzy Mathematical Morphology (FMM) (Bloch and Maître, 1995). The FMM has proven to be a solid theory and has been applied successfully in biomedical image segmentation (Kerre and Nachtegael, 2000; Blotta *et al.*, 2013, Bouchet *et al.*, 2007; Bouchet *et al.*, 2011; Gasparri *et al.*, 2011).

Operations between fuzzy sets are defined based on the conjunction and disjunction operators, applied to the membership values of these sets (Dubois and Prade, 1980). The values of the membership functions are numbers in the interval $[0,1]$. In most cases the images in gray levels are defined so that the gray level intensity at each pixel is an integer value belonging to the natural range $[\![0,255]\!]$. Therefore, to be able to apply the FMM operators, the gray level images must be modeled as fuzzy sets, with a change of scale to the range $[0,1]$. This process of scaling it is called "fuzzification", while the reverse process is called "desfuzzification". Usually the fuzzification function used, $g:\{0,1,2,...,255\}\to[0,1]$, is defined by:

$$g(x)=\frac{x}{255}, \tag{1}$$

The reverse process by which the intensities of the gray levels of an image, belonging to the interval $[0,1]$,

are brought back to the set $\{0,1,2,...,255\}$ is defined by the function $h:[0,1]\to\{0,1,2,...,255\}$ defined by:

$$h(x)=[255\ x], \tag{2}$$

where $[\bullet]:\mathbb{R}\to\mathbb{Z}$ represents the integer part function, defined by:

$$[a]=\sup\{k\in\mathbb{Z}/\,k\le a\}, \tag{3}$$

In the following sections μ and ν will denote two fuzzy sets, with membership functions $\mu:U\subset\mathbb{R}^2\to[0,1]$ and $\nu:U\subset\mathbb{R}^2\to[0,1]$, where the first one corresponds to a grayscale image and the second one determines the structuring element (SE). The membership functions are obtained by applying fuzzification function over the gray scale images.

The literature that studies the extension of basic operators in binary images to gray levels image using the fuzzy set theory presents several approaches, developed by various authors. Some of the authors which have developed several theories and have defined different formulas of the basic operators of the FMM are De Baets *et al.*, 1995; De Baets *et al.*, 1995; Kerre and Nachtegael, 2000; Bloch and Maître, 1995; Di Gesu *et al.*, 1993. Bloch y Maître have achieved the unification of all the models proposed by the authors mentioned previously, by the use of t-norms and s-norms. The following are the definitions of the basic operators of the FMM given by these authors.

Fuzzy dilation of the image μ by the SE ν (Bloch and Maître, 1995):

$$\delta(\mu,\nu)(x)=\sup_{y\in U}\left[t\left(\mu(y),\nu(y-x)\right)\right], \tag{4}$$

where $t(a,b)$ is a t-norm (Dubois and Prade, 1980). A function $t:[0,1]\times[0,1]\to[0,1]$ is a t-norm if it satisfies the following conditions, for every $a,b,c\in[0,1]$ (Dubois & Prade, 1980):

- boundary condition: $t(a,1)=a$
- symmetry: $t(a,b)=t(b,a)$
- monotonicity: If $a\le c$ and $b\le d$ then $t(a,b)\le t(c,d)$
- associativity: $t(t(a,b),c)=t(a,t(b,c))$

Fuzzy erosion of the image μ por el SE ν (Bloch and Maître, 1995):

$$\varepsilon(\mu,\nu)(x)=\inf_{y\in U}\left[s\left(\mu(y),c(\nu(y-x))\right)\right], \tag{5}$$

where $s(a,b)$ is a s-norm and $c(a)=1-a$ is the fuzzy complement operator (Klement *et al.*, 2004). A function $s:[0,1]\times[0,1]\to[0,1]$ is a s-norm if it satisfies the following conditions, for every $a,b,c\in[0,1]$ (Klement *et al.*, 2004):

- boundary condition: $s(a,0)=a$
- symmetry: $s(a,b)=s(b,a)$
- monotonicity: If $a\le c$ and $b\le d$ then $s(a,b)\le s(c,d)$
- associativity: $s(s(a,b),c)=s(a,s(b,c))$

A function $c:[0,1]\to[0,1]$ is a fuzzy complement if it satisfies the following conditions, for every $a,b\in[0,1]$ (Klement *et al.*, 2004):

- boundary condition: $c(0)=1$ and $c(1)=0$
- monotonicity: If $a\le b$ then $c(a)\ge c(b)$
- involutive property: $c(c(a))=a$

From these two operators the fuzzy opening, fuzzy closing and other fuzzy morphological operations can be defined.

Fuzzy opening of the image μ by the SE ν:

$$\gamma(\mu,\nu)=\delta(\varepsilon(\mu,\nu),\nu), \tag{6}$$

Fuzzy closing of the image μ by the SE ν:

$$\phi(\mu,\nu)=\varepsilon(\delta(\mu,\nu),\nu), \tag{7}$$

Similarly, others operators of the FMM can be derived from the classical definitions, substituting the basic operations by the equivalent fuzzy operations.

III. MATERIALS AND METHODS

The goal of this job is to compare classic and fuzzy morphological operators, regarding robustness against noise. An ideal robust morphological operator should provide similar results when applied to an image or the same image with additional noise. The degree of similarity between these two results measures the degree of robustness. Figure 1 shows the scheme of the experiments design.

We made two different experiments. The first one was designed to compare the robustness of the basic operators (dilation and erosion). The second one was designed to compare the robustness of the morphologicla filters (aperture and closing).

A. Experiment for basic operators

For the first comparison, based on dilation, we applied the morphological operators, classic and fuzzy, to the two groups of images: a) without noise, and b) with varied levels of noise. The resulting images were compared, noiseless versus noisy ones, using the mean square error as a measure of dissimilarity. We used 6 fuzzy operators (using the t-norms and s-norms listed in Tables 1 and 2, respectively) and 6 levels of noise

(independent Gaussian noise with mean zero and increasing variance). Each comparison was repeated 100 times, using different realizations of the random noise, and the resulting were averaged.

The main source of noise in the magnetic resonance imaging (MRI) is the thermal noise in the receiver and the body noise. The body noise is originated in the random fluctuations of the spins that induce the voltage in the receiving antenna. In a well designed high-field MRI system, the body noise dominates over other sources of noise. This noise can be modeled as a Gaussian noise added to the MR signal. We used this type of noise to simulate noisy MR images (Carrión Pérez *et al.*, 2006).

The following list provides a detailed description of the experimental setup:

•*Images*: we used 10 magnetic resonance images (MRI), acquired with a Tesla 1.5. The protocol included coronal and axial images, weighted in T2 (TR/TE!/TE= 3,500/32/96 ms). We used this kind of images because of the noisy nature of these images. Figure 2 shows some examples of the images used for the analysis.

•*Noise*: we use independent Gaussian noise with distribution $N\left(0,\sigma^2\right)$. The 6 values of variance used were $\sigma^2 \in \{50,100,150,200,250,300\}$.

•*Iterations*: the analysis was repeated 100 times to average over the random generation of the random noise.

•*Parameters of the norms*: as seen in Tables 1 and 2, "Hamacher" and "Dubois & Prade" norms require an additional parameter. We used $\gamma = 0.2$. This value was determined heuristically.

•*Structuring elements*: For the MM flat SE of size 3×3, 5×5, 7×7, 11×11 and 15×15 were used. For the fuzzy operators 5 symmetric SE of the same size were used. They were the fuzzification of the flat SE of the MM (Fig. 3).

The experiments using erosion instead of dilation have the same settings, only replacing the morphological operators used.

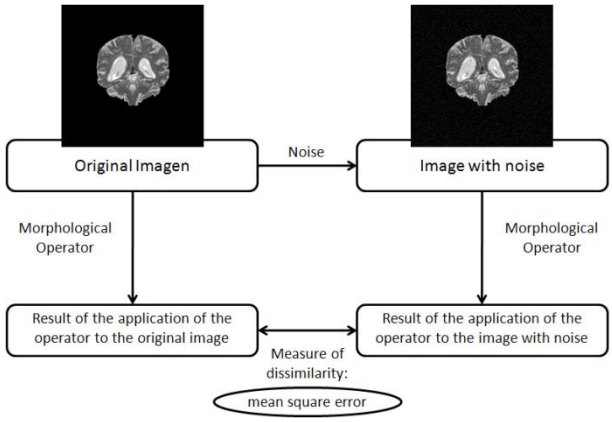

Figure 1: Scheme of the experiments design.

Table 1: Different kind of t-norms.

Standard	t_1	$t_1(a,b)=\min(a,b)$
Algebraic	t_2	$t_2(a,b)=a.b$
Bounded	t_3	$t_3(a,b)=\max(0,a+b-1)$
Drastic	t_4	$t_4(a,b)=\begin{cases}a & para\ \ b=1\\ b & para\ \ a=1\\ 0 & cc\end{cases}$
Dubois and Prade	t_5	$t_5(a,b)=\dfrac{a.b}{\max(a,b,\gamma)}$
Hamacher	t_6	$t_6(a,b)=\dfrac{a.b}{\gamma+(1-\gamma)(a+b-a.b)}$

Table 2: Different kind of s-norms.

Standard	s_1	$s_1(a,b)=\max(a,b)$
Algebraic	s_2	$s_2(a,b)=a+b-a.b$
Bounded	s_3	$s_3(a,b)=\min(1,a+b)$
Drastic	s_4	$s_4(a,b)=\begin{cases}a & para\ \ b=0\\ b & para\ \ a=0\\ 1 & cc\end{cases}$
Dubois and Prade	s_5	$s_5(a,b)=1-\dfrac{(1-a).(1-b)}{\max(1-a,1-b,\gamma)}$
Hamacher	s_6	$s_6(a,b)=\dfrac{a+b+(\gamma-2)a.b}{1+(\gamma-1)a.b}$

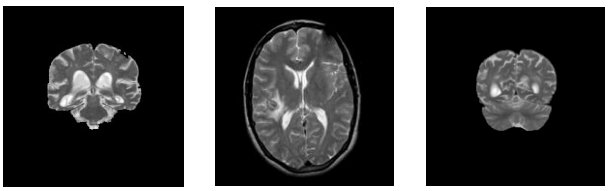

Figure 2: Examples of brain MRI used for the analysis of the basic morphological operators.

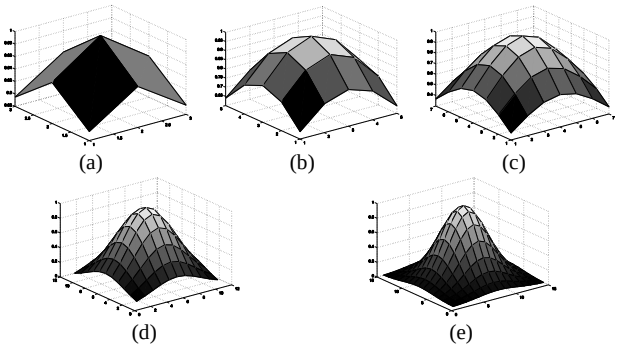

Figure 3: 3D view of the 5 structuring elements used for the FMM. (a) 3×3. (b) 5×5. (c) 7×7. (d) 11×11. (e) 15×15.

B. Experiments for morphological filters

To analyze the performance of the morphological filters we used a database of simulated magnetic resonance images, so that it was not necessary to add noise like in the previous experiments. The following

list provides a detailed description of the experimental setup:

• *Images:* We used 149 simulated magnetic resonance images (MRI). These images are the result of the work of scientists at the McGill University, who built a database of simulated images (BrainWeb: Simulated Brain Database) that contains a dataset of MRI, which are freely available in the web. In that work, the images were used to evaluate the performance of the techniques for MRI analysis. In those images, the pixels belonging to the different tissues are known a priori. The database consists of images, weighted in T1, with noise levels of 0%, 3%, 7% and 9%. Noise levels represent the percentage of standard deviation of the Gaussian noise with respect to the tissue signal (as a reference). The studies contains 181 slices of images of 217×181 pixels, taken at $1\,mm$ spacing and with $1\,mm^3$ of voxel volume. We used the slices ranged between 11 and 160. The remaining slices were discarded because they contain only bone information. Figure 4 shows some examples of the images used for the analysis.

• *FMM:* We used the six t-norms and s-norms listed in tables 1 and 2, respectively. In both cases, the basic operators, that define the aperture and closing, are based on a t-norm and its corresponding s-norm. For simplicity of notation, we use n_1 to denote the Standard norm, n_2 for the Algebraic norm, and so on.

To analyze the results under different conditions, we changed the dimension of the SE and made a choice for the value of the parameter γ, associated with some of the norms. We designed four experiments, including four SE and a values of γ, of the following form:

• *Structuring elements:* For the MM flat SE of size 3×3, 7×7, 11×11 and 15×15 were used. For the FMM symmetric SE of the same size were used. They were the fuzzification of the flat SE of the MM (Fig. 3).

•*Parameters of the norms:* as seen in Tables 1 and 2, "Hamacher" and "Dubois & Prade" norms require an additional parameter. We used $\gamma = 0.2$. This value was determined heuristically.

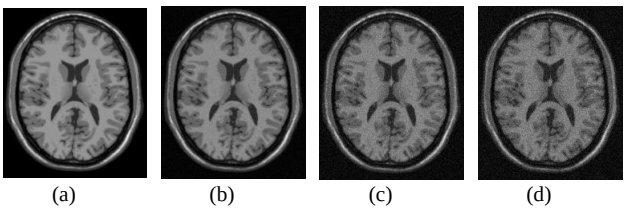

(a) (b) (c) (d)

Figure 4: Examples of MRI brain images used for morphological filters analysis. (a) Original image. (b) Image with 3% of noise. (c) Image with 7% of noise. (d) Image with 9% of noise.

III. RESULTS

This section presents the results obtained from the previously described experiments.

A. Results for basic operators experiment

Tables 3 to 6 show the lowest and highest errors, for dilation and erosion respectively, as function of the amount of noise (variance) and the operator used, t_1 to t_6 for the six t-norms, and s_1 to s_6 for the six s-norms, and MM for classic MM. The errors displayed are the average, over the 100 replications (100 realizations of noise) and nine images, of the MSE on the images.

Figure 5 shows graphically the box-plot of error rates comparing the classic mathematical morphology (MM) and the fuzzy morphology (FMM) based on the Bounded t-norm and s-norm, for both dilation and erosion, and for the largest amount of noise ($\sigma^2 = 300$), across all the structuring element sizes. Here we can see a significant decrease on error rates, or differences between the original and noisy images after application of the morphological operators.

Table 3: Lowest error for dilation. The name of the operators that reached the minimun is denoted between parentesis next to the error.

SE	σ^2		
	50	100	150
3×3	(t_3) 0.0031	(t_3) 0.00621	(t_3) 0.00968
5×5	(t_6) 0.00302	(t_3) 0.00624	(t_3) 0.00978
7×7	(t_6) 0.00295	(t_3) 0.00624	(t_3) 0.0098
11×11	(t_2) 0.00294	(t_3) 0.00625	(t_3) 0.00979
15×15	(t_2) 0.00292	(t_3) 0.00625	(t_3) 0.0098
SE	σ^2		
	200	250	300
3×3	(t_3) 0.01346	(t_3) 0.01755	(t_3) 0.02186
5×5	(t_3) 0.01369	(t_3) 0.0179	(t_3) 0.02233
7×7	(t_3) 0.01372	(t_3) 0.01789	(t_3) 0.0224
11×11	(t_3) 0.01369	(t_3) 0.01793	(t_3) 0.02244
15×15	(t_3) 0.01372	(t_3) 0.01794	(t_3) 0.02238

Table 4: Highest error for dilation. The name of the operators that reached the maximun is denoted between parentesis next to the error. No name is indicated when the maximum was reached by MM.

SE	σ^2		
	50	100	150
3×3	(t_4) 0.00398	0.00825	0.01306
5×5	(t_4) 0.00443	0.00886	0.01437
7×7	(t_4) 0.00444	0.00878	0.0144
11×11	(t_4) 0.00440	(t_4) 0.00845	0.01363
15×15	(t_4) 0.00439	(t_4) 0.00845	0.01327
SE	σ^2		
	200	250	300
3×3	0.01812	0.02344	0.02892
5×5	0.02037	0.02672	0.03323
7×7	0.02054	0.02698	0.03387
11×11	0.01964	0.02609	0.03285
15×15	0.01909	0.02531	0.0317

Table 5: Lowest error for erosion. The name of the operators that reached the minimun is denoted between parentesis next to the error.

SE	σ^2		
	50	100	150
3×3	(s_1) 0.00289	(s_3) 0.00599	(s_3) 0.00931
5×5	(s_1) 0.00272	(s_1) 0.0058	(s_3) 0.00911
7×7	(s_1) 0.00268	(s_1) 0.00571	(s_3) 0.00901
11×11	(s_1) 0.00267	(s_1) 0.00571	(s_3) 0.00898
15×15	(s_1) 0.00268	(s_1) 0.0057	(s_3) 0.00899
SE	σ^2		
	200	250	300
3×3	(s_3) 0.01298	(s_3) 0.01694	(s_3) 0.02117
5×5	(s_3) 0.01273	(s_3) 0.01666	(s_3) 0.02086
7×7	(s_3) 0.01259	(s_3) 0.01649	(s_3) 0.02065
11×11	(s_3) 0.01257	(s_3) 0.01646	(s_3) 0.02064
15×15	(s_3) 0.01257	(s_3) 0.01647	(s_3) 0.02062

Table 6: Highest error for erosion. The name of the operators that reached the maximun is denoted between parentesis next to the error. No name is indicated when the maximum was reached by MM.

SE	σ^2		
	50	100	150
3×3	(s_4) 0.0112	(s_4) 0.01512	(s_4) 0.01893
5×5	(s_4) 0.00824	(s_4) 0.0119	(s_4) 0.01548
7×7	(s_4) 0.00635	0.01232	0.0206
11×11	(s_4) 0.00614	0.01358	0.02285
15×15	(s_4) 0.00617	0.01358	0.02306
SE	σ^2		
	200	250	300
3×3	(s_4) 0.02264	(s_4) 0.02643	0.03083
5×5	0.02545	0.03334	0.04155
7×7	0.0294	0.03878	0.04847
11×11	0.033	0.04365	0.05514
15×15	0.03337	0.0445	0.05619

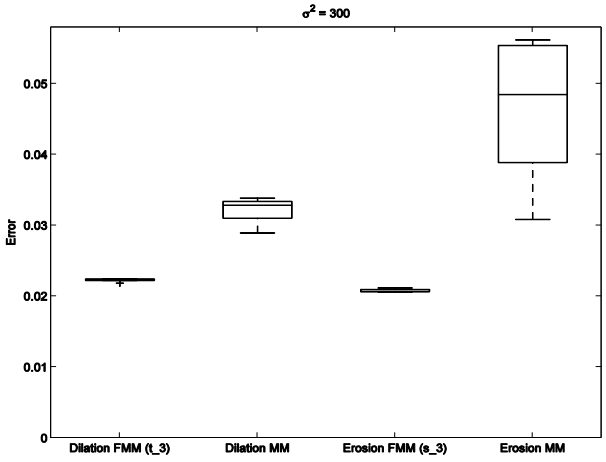

Figure 5: Box-plot of error rates comparing the classic mathematical morphology (MM) and the fuzzy morphology (FMM) based on the Bounded t-norm and s-conorm, for both dilation and erosion, and for the largest amount of noise ($\sigma^2 = 300$), across all the structuring element sizes.

B. Results for morphological filters experiment

Tables 7 to 10 show the lowest and highest errors, for opening and closing respectively, as function of the amount of noise and the operator used, n_1 to n_6 for the six norms, and MM for classic morphology. The mean square error was used as a measure of dissimilarity, to determine the quality of the operators, based on the results of the experiments. For every filter the error is computed by the following steps:

•Step 1: The mean square error is computed between the values of every pixel of the noiseless image and noisy image after the application of the filter.

•Step 2: The average of the pixel mean square error is computed for every cut (image).

•Step 3: The average and standard deviation of the errors is computed across all cuts (images) for each noise level.

Figure 6 show a scheme of the error computation process.

Figure 7 shows graphically the box-plot of error rates, comparing classic mathematical morphology (MM) against fuzzy morphology (FMM) based on different norms, for both opening and closing, and for the largest amount of noise (9%), across all the structuring element sizes.

Table 7: Lowest error for opening. The name of the operators that reached the minimun is denoted between parentesis next to the error.

SE	Noise Level		
	3%	7%	9%
3×3	(n_2) 0.00282	(n_2) 0.01117	(n_2) 0.01819
7×7	(n_6) 0.00222	(n_6) 0.00919	(n_6) 0.01494
11×11	(n_2) 0.00221	(n_3) 0.00913	(n_6) 0.01485
15×15	(n_6) 0.0022	(n_6) 0.00911	(n_6) 0.01481

Table 8: Highest error for opening. The name of the operators that reached the maximun is denoted between parentesis next to the error. No name is indicated when the maximum was reached by MM.

SE	Noise Level		
	3%	7%	9%
3×3	(n_5) 0.00413	0.01616	0.02589
7×7	0.00373	0.01691	0.0277
11×11	(n_4) 0.00341	0.0139	0.02294
15×15	(n_4) 0.00339	(n_4) 0.0119	0.01927

Table 9: Lowest error for closing. The name of the operators that reached the minimun is denoted between parentesis next to the error.

SE	Noise Level		
	3%	7%	9%
3×3	(n_6) 0.00201	(n_6) 0.00502	(n_6) 0.00732
7×7	(n_1) 0.00132	(n_5) 0.0029	(n_5) 0.00408
11×11	(n_1) 0.00117	(n_1) 0.00244	(n_5) 0.00341
15×15	(n_1) 0.00116	(n_1) 0.00241	(n_5) 0.00337

Table 10: Highest error for closing. The name of the operators that reached the maximun is denoted between parentesis next to the error.

SE	Noise Level		
	3%	7%	9%
3×3	(n_4) 0.00341	(n_4) 0.01197	(n_4) 0.01865
7×7	(n_4) 0.00341	(n_4) 0.01195	(n_4) 0.01861
11×11	(n_4) 0.00338	(n_4) 0.01186	(n_4) 0.01847
15×15	(n_4) 0.00333	(n_4) 0.0117	(n_4) 0.01824

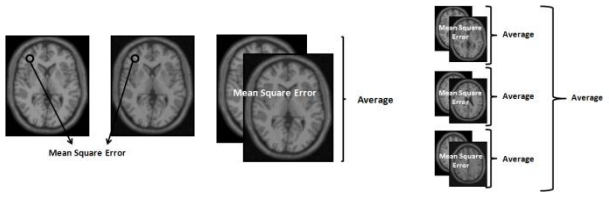

Figure 6: Scheme of the error computation for a whole set of images (a) Step 1. (b) Step 2. (c) Step 3.

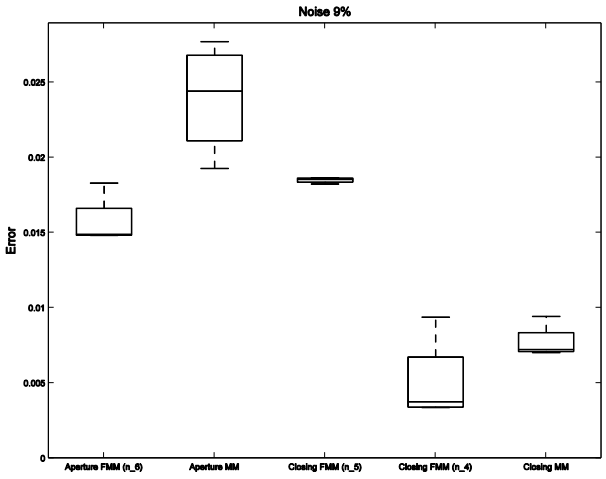

Figure 7: Error rates Box-plot comparing classic mathematical morphology (MM) against fuzzy morphology (FMM), based on different norms, for both opening and closing, and for the largest amount of noise (9%), across all the structuring element sizes.

III. DISCUSION

For the dilation experiments we can see that, for most of the cases, the MM operator has higher error than the MMD ones, and the differences increases for larger levels of noise. The erosion experiments show similar results, but with more MMD operators having worse performance than the MM operator for some conditions. In more than 70% of the cases, the worst FMM operators have better performance than the MM operators.

From the analysis of the results, we can conclude, in first place, that the Standard and Dubois & Prade norms have almost identical behavior. This is due to the fact that they definitions are similar, with identical behavior for most of the pixels. Second, we can see that the Bounded norm has the best performance (lowest error) for the images under study, and under the specific setup of the experiments.

For the erosion we can see that the error of the MM operator increase with the size of the structuring element (SE), behavior not replicated in the dilation experiment. This behavior of the erosion operators may indicate a sensibility issue: the larger the SE, the more sensible is the operator to noise.

From the results for opening, it is evident the for the images and noise under analysis, the Hamacher and Algebraic norms show the best performance for 3×3 structuring elements, and Hamacher alone shows best performance for other sizes of the structuring element.

It is important to note that the classic MM did not show always the worst performance, but just in two thirds of the cases. The other third of the cases present the Drastic and Dubois&Prade norms as worst performers.

In the results for closing, some MMD operators performed better than classic MM, while others performed worse. Hamacher norm showed the best performance, again, for 3×3 SE, while Bounded and Drastic norms showed the worse performance than MM. For 7×7, 11×11 and 15×15 SE, the worst performers were the same as in the 3×3, but the best performers were the Standard and Dubois&Prade norms. In all cases, MM was not the worst performer, neither the best performer.

III. CONCLUSIONS

Over all the range of settings, we can observe an overall better robustness, against noise, of MMD dilation and erosion operator against MM operators. Noise present in the images affects less the MMD than the MM operators. Under the experimental conditions used for this work, some morphological filters (opening and closing) show more robustness, to noise in the images, when using fuzzy mathematical morphology than when using classic mathematical morphology.

Future works, focused on extending the results and knowledge on the behavior of the MMD operators, include the comparison of morphological filters, designed to remove the existing noise, and the study of the effect of the structuring element on the filters.

REFERENCES

Bangham, J. A. and S. Marshall, "Image and Signal processing with mathematical morphology", *IEE Electronics & Communication Engineering Journal*, **10**, 117-128 (1998).

Bloch, I. and Maître, H., "Fuzzy mathematical morphologies: A comparative study", *Pattern Recognition*, **28**, 1341-1387 (1995).

Blotta E., A. Bouchet, M. Brun, V. Ballarin, "Characterization of bio-dynamic speckles through classical and fuzzy mathematical morphology tools", *Signal Processing, Elsevier*. Available online 1 February 2013, 10.1016/j.sigpro.2013.01.001.

Bouchet, A., J. Pastore, V. Ballarin, "Segmentation of Medical Images using Fuzzy Mathematical Morphology", *Journal of Computer Science and Technology*, **7**, 256-262 (2007).

Bouchet, A., J. Pastore, R.E. Andrade, M. Brun, V. Ballarin, "Compensatory Logic applied to Digital Image Processing", in: *Towards a trans-disciplinary technology*

of Business and Organizational Intelligence: Gathering Knowledge Discovery, Knowledge Management and Decision, R.E. Andrade, J.M. Gómez, A.R. Valdéz, (Eds.), Shaker Verlag, Aachen, University of Oldenburg, Alemania, 226-239 (2011).

Carrión Pérez, P., J. Ródenas García, J.J. Rieta Ibañez, *Ingeniería biomédica: Imágenes médicas*, Ediciones de la Universidad de Castilla-La Mancha, España (2006).

De Baets, B., E. Kerre, M. Gupta, "The Fundamentals of Fuzzy Mathematical Morphology. Part 1: Basic Concepts", *International Journal of General Systems*, **23**, 155-171 (1995).

De Baets, B., E. Kerre, M. Gupta, "The Fundamentals of Fuzzy Mathematical Morphology. Part 2: Idempotence, Convexity and Decomposition", *International Journal of General Systems*, **23**, 307-322 (1995).

Di Gesu, V., M. C. Maccarone, M. Tripiciano, "Mathematical Morphology based on Fuzzy Operators", in: *Fuzzy Logic*, R. Lowen and M. Roubens, Eds., Kluwer Academic Publishers, 477-486 (1993).

Dubois, D. and H. Prade, *Fuzzy Sets and Systems: Theory and Applications*, Academic Press Inc, New York (1980).

Gasparri, J.P., A. Bouchet, G. Abras, V. Ballarin, J.I. Pastore, "Medical Image Segmentation using the HSI color space and Fuzzy Mathematical Morphology", *Journal of Physics: Conference Series*, **332**, 1-9 (2011).

Kerre, E. and M. Nachtegael, *Fuzzy Techniques in Image Processing*, **52**, New York (2000).

Klement, E.P., R. Mesiar, E. Pap., "Triangular norms. Position paper I: basic analytical and algebraic properties", *Fuzzy Sets and Systems*, **143**, 5-26 (2004).

Ronse, C. and H. Heijmans, "The algebraic basis of mathematical morphology : II. Openings and closings", *Computer Vision, Graphics, and Image Processing: Image Understanding*, **54**, 74-97 (1991).

Serra, J, *Image analysis and mathematical morphology*, **1**, Academic Press, London (1982).

Serra, J., *Image analysis and mathematical morphology*, **2**, Academic Press, London (1988).

Zadeh, L. A., "Fuzzy sets", *Information and Control*, **8**, 338-353 (1965).